International Journal of Multimedia and Ubiquitous Engineering
Vol.11, No.7 (2016), pp.291-300
http://dx.doi.org/10.14257/ijmue.2016.11.7.29

Medical Image Fusion via Non-Subsampled Contourlet Transform

Niu Ling[1] and Qi Yingchun[2]

[1]*Zhou Kou Normal University, Zhoukou 466001, China;*
suncoco_nl@163.com
[2]*Zhoukou Normal University, Zhoukou Henan Province, 466001, China*
E-mail: Qiyingchun@163.com

Abstract

Due to the obvious advantages, the technology of medical imaging has been widely utilized in the medical areas. Commonly, the medical images of different imaging mechanism are able to guide the radiologist for the precise diagnosis of disease and for more effective interventional treatment procedures. Consequently, the fusion of different medical images of the same scene is necessary. This paper proposes a novel fusion technique for medical images based on non-subsampled contourlet transform (NSCT). Due to the better competence of image information capturing, NSCT is utilized to conduct the multi-scale and multi-directional decompositions of source images. In addition, the models of both region average energy and region coefficient deviation are used for the fusion for low-frequency sub-images and high-frequency ones, respectively. In comparison with several current typical fusion techniques, the proposed one has remarked superiorities in terms of both subjective and objective evaluations.

Keywords*: non-subsample contourlet transform, image fusion, region average energy, region coefficient deviation*

1. Introduction

The technology of image fusion has been widely utilized in the medical fields. Commonly, the image from different imaging sensors owns specific information about the human body and the same is not available with other imaging modality. For example [1], computed tomography (CT) images provides electron density map required for accurate radiation dose estimation and superior cortical bone contrast; however, it is limited in soft tissue contrast. Magnetic resonance imaging (MRI) provides excellent soft tissue contrast which permits better visualization of tumors or tissue abnormalities in different parts of the body. But MRI has lack of signal from cortical bone and has image intensity values that have no relation to electron density. For the precise diagnosis of disease and for more effective interventional treatment procedures, radiologists need the information from two or more imaging modalities. For this purpose, the multimodal medical image fusion has been identified as a promising solution which aims to integrating information from multiple modality images to obtain a more complete and accurate description of the same object.

Recently, a great number of fusion techniques [2-10] for images have been proposed by scholars both at home and abroad. The well-known pixel level fusion is based on principal component analysis (PCA), independent component analysis (ICA), contrast pyramid (CP), gradient pyramid (GP) filtering, *etc.* However, the above mentioned ones are not suitable for medical image fusion. The wavelet transform (WT) [11-12] replaced the pyramid transform to be the mainstream fusion technique for images. However, the better capture performance of WT can only be achieved in terms of horizontal, vertical and diagonal directions; furthermore, the singular information of lines cannot be captured. Several years later, several other transform domain techniques for image fusion, such as

ISSN: 1975-0080 IJMUE

ridgelet transform [13], curvelet transform [14-15] and contourlet transform [16-17], appear in succession so that the fusion property has been greatly enhanced. Contourlet is a "true" 2-D sparse representation for 2-D signals like images where sparse expansion is expressed by contour segments. As a result, it can capture 2-D geometrical structures in visual information much more effectively than traditional multiscale methods. Compared with the former patterns, non-subsampled contourlet transform (NSCT) [18-20] has obvious priorities in terms of information capturing, so it gradually becomes the mainstream and a hot research object in the field of medical image fusion.

Based on the above, a novel medical image fusion based on NSCT is proposed in this paper. Firstly, the multi-scale and multi-directional decompositions of source images can be conducted to produce a low-frequency sub-image and a series of high-frequency sub-images. Then, the models of both region average energy and region coefficient deviation are used for the fusion for low-frequency sub-images and high-frequency ones, respectively. Finally, the inverse NSCT is adopted to produce the final fusion resultant image.

The remaining paper is organized as follows: Section 2 gives brief overview of NSCT. Section 3 describes the proposed fusion rules in detail. Experimental results and relative analysis are presented in Section 4. Section 5 gives the conclusions.

2. Non-Subsampled Contourlet Transform

NSCT [21], based on the theory of contourlet transform, is a kind of multi-scale, multi-directional computation framework of discrete images. The whole course of NSCT is still composed of two stages including multi-scale analysis and multi-directional analysis, which are similar to those of CT. The main difference lies in that, in the course of decomposition and reconstruction, traditional upsamplers and downsamplers in CT do not exist in NSCT anymore, so that the NSCT is a fully multi-scale, multi-directional, good time-frequency property and shift-invariant expansion.

NSCT falls into two phases including non-subsampled pyramid (NSP) and non-subsampled directional filter bank (NSDFB). The former phase ensures the multi-scale property by using two-channel non-subsampled filter bank, and a low-pass image with a band-pass one can be produced at each NSP decomposition stage. The subsequent NSP decomposition stages are carried out to decompose the low-pass component available iteratively to capture the singularities in the image. As a result, NSP can result in k+1 sub-band images including one low-pass image and k band-pass images whose sizes are all the same as that of the source image, where k denotes the number of decomposition stages. Figure 1 gives the NSP decomposition with k=3 stages. The NSDFB, constructed by combining the directional fan filter banks devised by Bamberger and Smith [22], is two-channel non-subsampled filter banks. NSDFB allows the direction decomposition with l stages in band-pass images from NSP at each scale and produces 2^l directional sub-band images which have the same size as the source image. Thus the NSDFB endows the NSCT with the multi-direction property and we can benefit a lot from the NSDFB because it provides us with more precise directional detail information. A four-channel non-subsampled directional filter bank constructed with two-channel fan filter banks is illustrated in Figure 2.

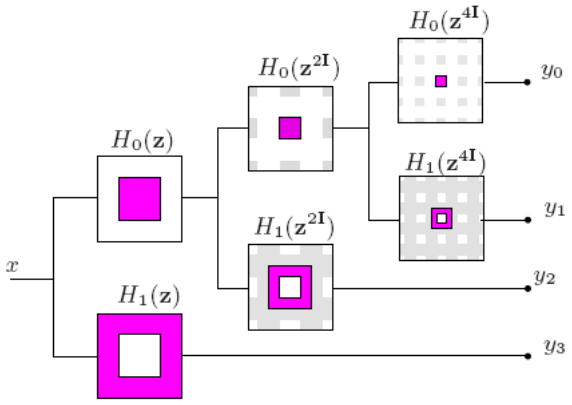

Figure 1. A Three-Stage Nonsubsampled Pyramid Decomposition

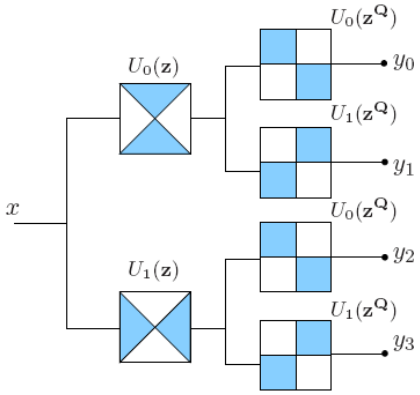

Figure 2. A Four-Channel Nonsubsampled Directional Filter Bank

3. Proposed Fusion Rules

3.1. Fusion of Low-Frequency Sub-Images

Low-frequency sub-band is smoothed version of original image. It represents the outline of the image. There are several current methods as follows. One method is conducted like this: when given several source images, certain image's low-frequency component whose spectrum property is the best is directly regarded as the low- frequency component of the fused image. The second method is also easy. Give the source images' low-frequency components the same weight values and fuse them to obtain the low-frequency component of the final fused image. The third one is called adaptive weighted values method. The weighted values of source images' low-frequency components are adaptively determined according to several statistical eigenvalues. As the number of decomposition levels are restricted to two in this work, most of the signal energy and few details of the original image still present in the low-frequency sub-images. Hence, it is important fuse the low-frequency sub-images in such a way to retain both the detailed information as well as approximate information present in it. In the proposed method,

In this paper, a new fusion technique based on the region average energy is presented. The concrete procedures can be described as follows:

(i) The window size can be fixed according to the complexity extent of the image, usually a square region with the size $n \times n$ can be chosen. Where n is an odd number not less than three. The region average energy can be obtained like this:

$$E'_x(x,y)=\frac{1}{n\times n}\sum_{m=-(n-1)/2}^{m=(n-1)/2}\sum_{r=-(n-1)/2}^{r=(n-1)/2}c^2(x+m,y+r) \tag{1}$$

Where $E'_x(x, y)$ is the low-pass region average energy of the pixel (x, y), x denotes the infrared image or the intensity component image of the visible light image, c is the coefficient of the low-pass component.

(ii) A coefficient called the match degree which can describe the match extent of the corresponding region average energy in the two images is calculated:

$$M(x,y)=\frac{2}{E'_{V\_I}+E'_{IR}}\times\sum_{m=-(n-1)/2}^{m=(n-1)/2}\sum_{r=-(n-1)/2}^{r=(n-1)/2}c_{V\_I}(x+m,y+r)\cdot c_{IR}(x+m,y+r) \tag{2}$$

(iii) According to the mathematical knowledge:

$$0\le M(x,y)\le n^2 \tag{3}$$

In order to compare the match degrees of the two images conveniently, it is necessary to range the degrees in the interval [0, 1], and the match degree can be represented like this:

$$M'(x,y)=\frac{2}{n^2\left(E'_1+E'_2\right)}\times\sum_{m=-(n-1)/2}^{m=(n-1)/2}\sum_{r=-(n-1)/2}^{r=(n-1)/2}c_1(x+m,y+r)\cdot c_2(x+m,y+r) \tag{4}$$

The match degree can describe the similarity extent of the corresponding pixels in two images, the larger the value of $M'(i, j)$ is, the more similar the corresponding pixels in the two images are.

(iv) The weight values of the two images' low-frequency components can be decided according to the value of $M'(i, j)$. In this paper, a predefined threshold λ is used to compare with $M'(i, j)$. The coefficient of the low-frequency component of the fusion image can be fixed as follows:

$$C_F(x,y)=\begin{cases}C_1(x,y), & if\ M'(x,y)\le\lambda\ and\ E'_1(x,y)\ge E'_2(x,y)\\ C_2(x,y), & if\ M'(x,y)\le\lambda\ and\ E'_2(x,y)\ge E'_1(x,y)\\ 0.5\times(C_1(x,y)+C_2(x,y)), & if\ M'(x,y)>\lambda\end{cases} \tag{5}$$

Where the subscripts namely "1" and "2" denote the two images. F is the fused image.

3.2. Fusion of High-Frequency Sub-Images

High-frequency sub-images represent the detailed component of the source images such as edges, contours, and object boundaries, so the fusion rules of the band-pass component play a very important role in the whole course of image fusion. The most commonly used fusion rule for high-frequency sub-band is selecting the coefficient having absolute maximum value. But this scheme is sensitive to noise and also there is possibility to lose some important information as the coefficient selection is based on single coefficient value without considering neighbouring coefficients. Another scheme used is coefficient selection based on activity level measurement value.

Unlike most schemes proposed before, we will utilize the model of region coefficient deviation to conduct the fusion of high-frequency sub-images.

(i) We develop a new norm called "region coefficient deviation" in this paper, and it becomes one of the indexes of the band-pass component coefficient fusion:

$$\left\|e_x(x,y)\right\|_{n\times n}=\sum_{m=-(n-1)/2}^{m=(n-1)/2}\sum_{r=-(n-1)/2}^{r=(n-1)/2}\left|\,\|e_x(x+m,y+r)\|-e'(x,y)_{n\times n}\,\right| \tag{6}$$

Where $e'(x, y)_{n\times n}$ is the average value of the absolute values of the band-pass coefficients, and its expression is as follows:

$$e'(x,y)_{n\times n} = \frac{1}{n^2}\sum_{m=-(n-1)/2}^{m=(n-1)/2}\sum_{r=-(n-1)/2}^{r=(n-1)/2} |e_x(x+m,y+r)| \tag{7}$$

Where the subscript x denotes the intensity component image of the visible light image or the infrared image, e is the coefficient of the band-pass component.

(ii) Since the information entropy can illuminate the information quantities of the image and its distribution, the information entropy can also become an index guiding the fusion of the high-frequency coefficients, whose expression is:

$$\left\|En_x(x,y)\right\|_{n\times n} = -\sum_{m=-(n-1)/2}^{m=(n-1)/2}\sum_{r=-(n-1)/2}^{r=(n-1)/2} f_x(x+m,y+r)\ln f_x(x+m,y+r) \tag{8}$$

Where f denotes the gray value of the pixel.

(iii) The fusion principle of the high-frequency component coefficients is established as follows:

$$e_F(x,y) = \begin{cases} e_1(x,y), & if \left\|e_1(x,y)\right\|_{n\times n} > \left\|e_2(x,y)\right\|_{n\times n} \\ e_2(x,y), & if \left\|e_1(x,y)\right\|_{n\times n} < \left\|e_2(x,y)\right\|_{n\times n} \\ e_1(x,y), & if \left\|e_1(x,y)\right\|_{n\times n} = \left\|e_2(x,y)\right\|_{n\times n} \ and \ En_1(x,y) \geq En_2(x,y) \\ e_2(x,y), & if \left\|e_1(x,y)\right\|_{n\times n} = \left\|e_2(x,y)\right\|_{n\times n} \ and \ En_1(x,y) < En_2(x,y) \end{cases} \tag{9}$$

Where the subscripts namely "1" and "2" denote the two images. F is the fused image.

4. Experimental Results and Analysis

Some general requirements for fusion algorithm are: (1) it should be able to extract complimentary features from input images. (2) it must not introduce artifacts or inconsistencies according to Human Visual System and (3) it should be robust and reliable. Generally, these can be evaluated subjectively or objectively. The former relies on human visual characteristics and the specialized knowledge of the observer, hence vague, time-consuming and poor-repeatable but are typically accurate if performed correctly. For verifying the practical performance of the proposed technique, we utilize the MATLAB software to emulate, compare and analyze the fusion results of several compared fusion techniques and the proposed technique.

4.1. Experimental Condition

Simulation experiments are carried out in a PC with Windows 7/2.4GHz/4G. In this section, we select different kinds of original images with four imaging mechanisms to carry out the experiments, which are referred to CT, MRI, fluid attenuated inversion recovery (FLAIR) and diffusion weighted (DW) images. And two pairs of original images' size are all 512×512. Moreover, we choose three techniques comparing with the novel technique, including the coupling of multi-channel pulse neural network technique (technique 1) [23], shearlet transform technique (technique 2) [24] and Laplace transform (technique 3) [25]. In order to assure the objectivity of fusion results, all the parameters in technique 1, 2 and 3 are also the existing set mode's values in references.

Furthermore, the performance evaluation' ways as to the ending fusion results are subjective visible evaluation and objective index values evaluation. And Information Entropy (IE), Edge Intensity (EIN), and Image Definition (ID) are chosen to be evaluation index. The index value of IE denotes the quantity of information in image. And the bigger are the values, the information in fusion images are ampler. The index value of EIN reflects the keeping extent of the edge features information in the image, so its value is in

direct proportional to the amount of the edge information. Similarly, ID represents the definition level of the whole image. This is to say the bigger the value of ID, the higher the definition level of the image.

4.2. Experimental Results and Analysis

The two pairs of source images are shown in Figure 3. Obviously, each image has its specific characteristics. For example, in CT image, whose intensity is related to the issue density, bones can reflect a much higher intensity, while other things such as the parenchyma often cannot achieve sufficient description in it. Coincidently, MRI images own the opposite property against that of CT images.

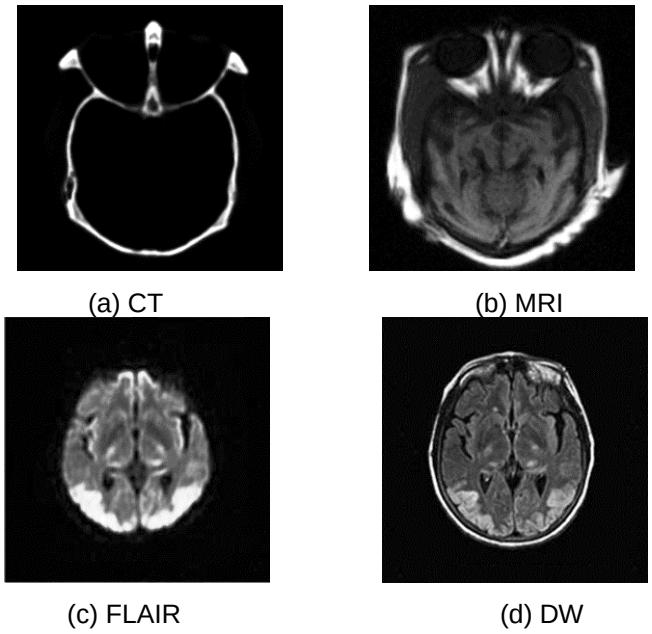

(a) CT (b) MRI

(c) FLAIR (d) DW

Figure 3. Original Source Images

Figure 4 and Figure 5 give the fusion results of the four techniques towards the two groups of source images. Observed from the results, the fused image based on techniques 1 has obvious artifacts, such as the area of the top right corner. Similarly, the fused results based on technique 2 and technique 3 cannot extract the main information from source images and fused it in the results. For example, in Figure 4, the information in MRI is not well included in fused results. Instead, the image based on the proposed technique has better visual effects.

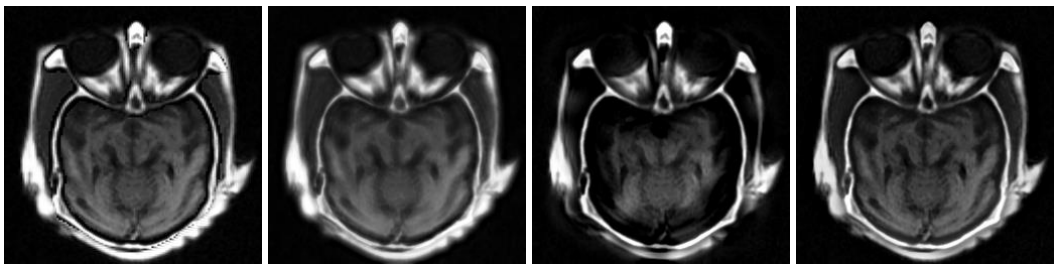

(a) Fusion Results of Technique 1 (b) Fusion Results of Technique 2 (c) Fusion Results of Technique 3 (d) Fusion Results of The Proposed Technique

Figure 4. Fusion Results of the First Group Source Images

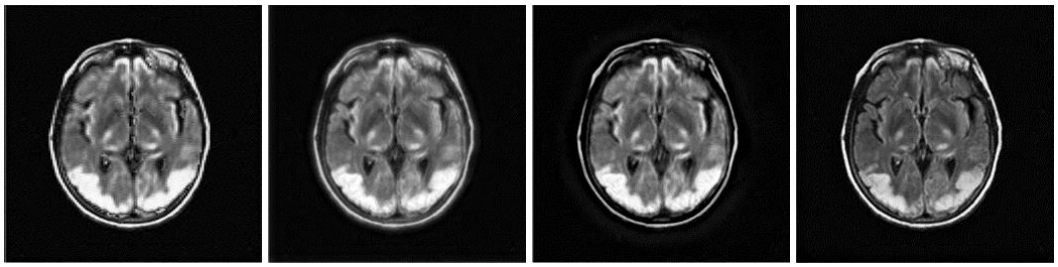

(a) Fusion Results of Technique 1 (b) Fusion Results of Technique 2 (c) Fusion Results of Technique 3 (d) Fusion Results of The Proposed Technique

Figure 5. Fusion Results of the Second Group Source Images

4.3. Discussions

In order to further compare the fusion performance of the four techniques, this section will introduce another group of medical images to conduct the fusion course, which is shown in Figure 6, and the fused results are given in Figure 7.

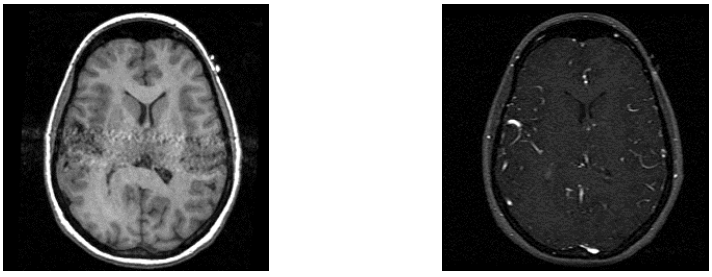

(a) Image 1 (b) Image 2

Figure 6. Another Group of Medical Images

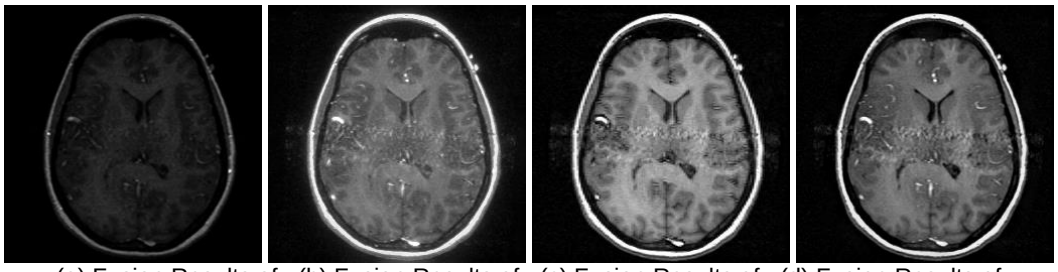

(a) Fusion Results of Technique 1 (b) Fusion Results of Technique 2 (c) Fusion Results of Technique 3 (d) Fusion Results of The Proposed Technique

Figure 7. Fusion Results of the First Group Source Images

Besides, the results in Figure 4 and Figure 5 are used to compare with the original source images, whose results are shown in Figure 8-11. Obviously, more information the contents has, better fused effects the technique is. According to the results, the proposed technique has distinct superiorities over those based on other three ones.

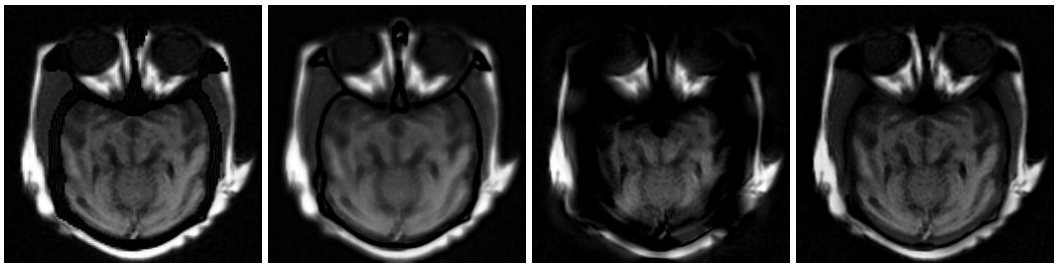

(a) Comparison Result of Technique 1 (b) Comparison Result of Technique 2 (c) Comparison Result of of Technique 3 (d) Comparison Result of The Proposed Technique

Figure 8. Comparison Results with Figure 3 (a)

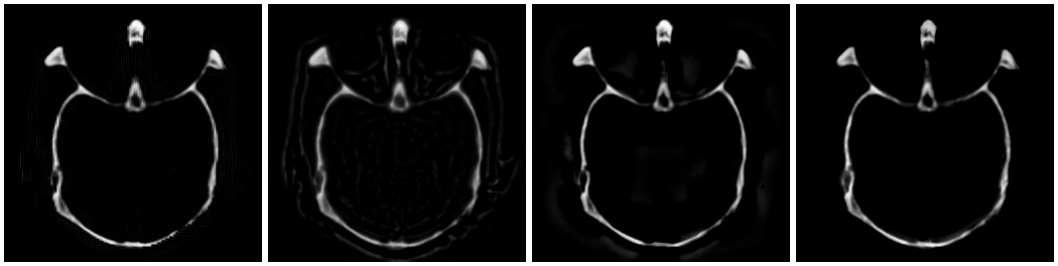

(a) Comparison Result of Technique 1 (b) Comparison Result of Technique 2 (c) Comparison Result of Technique 3 (d) Comparison Result of The Proposed Technique

Figure 9. Comparison Results with Figure 3 (b)

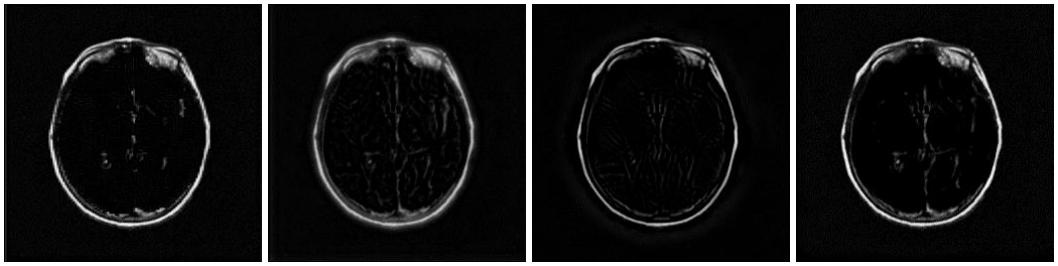

(a) Comparison Result of Technique (b) Comparison Result of Technique 2 (c) Comparison Result of Technique 3 (d) Comparison Result of The Proposed Technique

Figure 10. Comparison Results with Figure 3 (c)

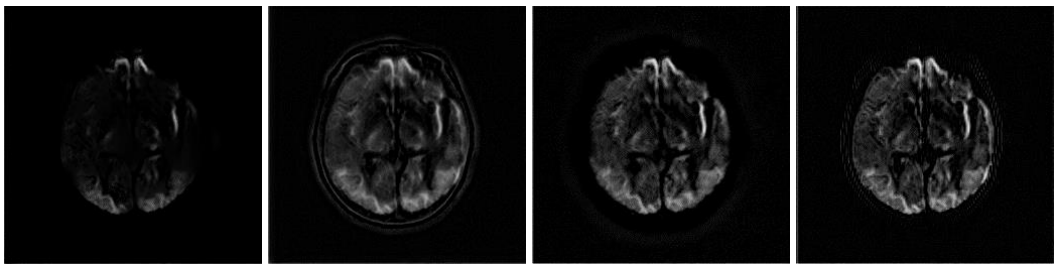

(a) Comparison Result of Technique 1 (b) Comparison Result of Technique 2 (c) Comparison Result of Technique 3 (d) Comparison Result of The Proposed Technique

Figure 11. Comparison Results with Figure 3 (d)

5. Conclusion

In this paper, a novel image fusion framework is proposed for medical image fusion, which is based on non-subsampled contourlet transform. For fusion, two models are presented to effectively complete the fusion course of low-frequency and high-frequency sub-images. In our experiment, several groups of medical images are fused using

conventional fusion algorithms and the proposed framework. The comparisons demonstrate that the proposed algorithm can enhance the details of the fused image, and can improve the visual effect with much less information distortion than its competitors.

Acknowledgements

The authors thank the anonymous reviewers and editors for their invaluable suggestions. The work was supported in part by the Key scientific research projects of Henan Province of China under Grant 16A520104, in part by the Science and technology project of Henan Province of China under Grant 152102210367, in part by the soft science research project of Henan province of China under Grant 142400411133.

References

[1] P. Ganasala and V. Kumar, "CT and MR image fusion scheme in nonsubsampled contourlet transform domain", Journal of Digit Imaging, vol. 27, no. 3, **(2014)**, pp. 407-418.
[2] Q. Guihong, Z. Dali and Y. Pingfan, "Medical image fusion by wavelet transform modulus maxima", Optical Express, vol. 9, **(2001)**, pp. 184-190.
[3] V. Barra and J. Y. Boire, "A general framework for the fusion of anatomical and functional medical images", Neuroimage, vol. 13, no. 3, **(2001)**, pp. 410-424.
[4] L. Yang, B. L. Guo, and W. Ni, "Multimodality medical image fusion based on multiscale geometric analysis of contourlet transform", Neurocomputing, vol. 72, **(2008)**, pp. 203-211.
[5] F. E. Ali, I. M. El-Dokany, A. A. Saad and F. E. A. E. Samie, "Curvelet fusion of MR and CT images", Progress in Electromagnetics Research C, vol. 3, **(2008)**, pp. 215-224.
[6] N. Boussion, M. Hatt, F. Lamare, C. C. L. Rest and D. Visvikis, "Contrast enhancement in emission tomography by way of synergistic PET/CT image combination", Computer Methods and Programs in Biomedicine, vol. 90, no. 3, **(2008)**, pp. 191-201.
[7] S. Daneshvar and H. Ghassemian, "MRI and PET image fusion by combining IHS and retina-inspired models", Information Fusion, vol. 11, no. 2, **(2010)**, pp. 114-123.
[8] Y. Yang, D. S. Park, S. Huang and N. Rao, "Medical image fusion via an effective wavelet-based approach", Eurasip Journal on Advances in Signal Processing, vol. 1, **(2010)**, pp. 1-13.
[9] S. Das, M. Chowdhury and M. K. Kundu, "Medical image fusion based on ripplet transform type-I", Progress in Electromagnetics Research B, vol. 30, **(2011)**, pp. 355-370.
[10] T. Li and Y. Wang, "Biological image fusion using a NSCT based variable- weight method", Information Fusion, vol. 12, no. 2, **(2011)**, pp. 85-92.
[11] Y. C. Yang, J. W. Dang and Y. P. Wang, "A Medical Image Fusion Method Based on Lifting Wavelet Transform and Adaptive PCNN", Journal of Computer-aided Design & Computer Graphics, vol. 24, no. 4, **(2004)**, pp. 494-499.
[12] Z. P. Xu, "Medical image fusion using multi-level local extrema", Information Fusion, vol. 19, no. 1=, 38-48 **(2014)**
[13] W. Q. Wang, L. C. Jiao and S. Y. Yang, "Fusion of multispectral and panchromatic images via sparse representation and local autoregressive model", Information Fusion, vol. 20, no. 1, **(2014)**, pp. 73-87.
[14] J. Tian and L. Chen, "Adaptive multi-focus image fusion using a wavelet-based statistical sharpness measure", Signal Processing, vol. 92, no. 9, **(2012)**, pp. 2137-2146.
[15] Y. A. Zheng, J. S. Song, W. M. Zhou and R. H. Wang, "False Color Fusion for Multi-band SAR Images Based on Contourlet Transform", Acta Automatica Sinica, vol. 33, no. 4, **(2007)**, pp. 337-341.
[16] G. S. Hu, D. Liao and J. Kong, "Remote Sensing Image Fusion Based on Support Vector Value Contourlet Transform", Acta Electronica Sinica, vol. 38, no. 6, **(2010)**, pp. 1287-1292.
[17] J. H. Adu, J. H. Gan, Y. Wang and J. Huang, "Image fusion based on non-subsampled contourlet transform for infrared and visible light image", Infrared Physics & Technology, vol. 61, no. 1, **(2013)**, pp. 94-100.
[18] A. L. Cunha, J. P. Zhou and M. N. Do, "Non-subsampled contourlet transform: filter design and applications in denoising", Proceeding Int. Conf. Image Processing, Genova, Italy, **(2005)**, pp. 749-752.
[19] J. P. Zhou, A. L. Cunha and M. N. Do, "Non-subsampled contourlet transform: construction and application in enhancement", Proceeding Int. Conf. Image Processing, Genova, Italy, **(2005)**, pp. 469-472.
[20] A. L. Cunha, J. P. Zhou and M. N. Do, "The non-subsampled contourlet transform: Theory, design, and applications", IEEE Transactions on Image Processing, vol. 15, no. 10, **(2006)**, pp. 3089-3101.
[21] W. W. Kong, Y. J. Lei, Y. Lei and S. Lu, "Image Fusion Technique Based on NSCT and Adaptive Unit-Fast-Linking PCNN", IET Image Processing, vol. 5, no. 2, **(2011)**, pp. 113-121.
[22] R. H. Bamberger and M. J. T. Smith, "A filter bank for the directional decomposition of images: Theory and design", IEEE Transactions on Signal Processing, vol. 40, no. 4, **(1992)**, pp. 882-893.

[23] Z. B. Wang and Y. D. Ma, "Medical image fusion using m-PCNN", Information. Fusion, vol. 9, no. 2, **(2008)**, pp. 176-185.
[24] Q. G. Miao, C. Shi, P. F. Xu, M. Yang and Y. B. Shi, "A novel algorithm of image fusion using shearlets", Optics Communication, vol. 284, no. 6, **(2011)**, pp. 1540-1547.
[25] P. Burt and E. Adelson, "The laplacian pyramid as a compact image code", IEEE Transactions on Communications, vol. 31, no. 4, **(1983)**, pp. 532-540.

Author

Niu Ling, received the B. Eng degree in Computer science from Henan normal university and M. Eng degree in Computer science from Chengdu University of Technology. She is currently researching on computer application technology.

Qi Yingchun, born on Jan. 10, 1963, Henan Province, China. Current position, grades: Associate Professor of Zhoukou Normal University. University studies: computer application technology, Scientific interest: network of computer.

